# Fragment production in proton–induced reaction on $^{209}$Bi target at intermediate energy range

A. R. Balabekyan,[1] G. S. Karapetyan,[2] E. Andrade-II,[3] A. Deppman,[4] S. V. Gaginyan,[1] E. Melyan,[1] J. R. Drnoyan,[5] V. I. Zhemenik,[5] J. Adam,[5] L. Zavorka,[5] A. A. Solnyshkin,[5] V. M. Tsoupko-Sitnikov,[5] J. Khushvaktov,[5] and E. B. Hernández[3]

[1]*Yerevan State University, A. Manoogian, 1, 025, Yerevan, Armenia*

[2]*CCNH, Universidade Federal do ABC 09210-580, Santo Andre, Brazil*

[3]*Departamento de Ciências Exatas e Tecnológicas, Universidade Estadual de Santa Cruz, Ilhéus, BA, Brazil*

[4]*Instituto de Fisica, Universidade de São Paulo, P. O. Box 66318, 05389-970 São Paulo, SP, Brazil*

[5]*Joint Institute for Nuclear Research (JINR), Laboratory of Nuclear Problems (LNP), Joliot-Curie 6, Dubna 141980, Moscow region, Russia*

(Received 25 June 2019; revised manuscript received 20 July 2019; published 19 August 2019)

We used the phasotron of the Laboratory of Nuclear Problems at JINR to irradiate isotopically pure $^{209}$Bi target with 660 MeV protons. Cross sections of the fragment production with mass numbers $24 \leqslant A \leqslant 210$ u were measured for the first time using the direct $\gamma$-spectrometry method with a high-resolution HpGe detector. The $\gamma$ lines of the fragments have been identified, and the cross sections determined by the DEIMOS code. The results of the measured nuclide cross section have been parametrized in terms of a three-parameter equation in order to reproduce the real isobaric distribution. Fission and spallation mass yields have been reconstructed on the base of charge distribution of reaction products. The main reaction results have been compared with other experimental data obtained from the proton-induced reaction at 600 MeV as well as with theoretical model calculations using the CRISP code.

DOI: 10.1103/PhysRevC.100.024616

## I. INTRODUCTION

In spite of the fact that reactions induced by protons of energies between hundreds of MeV and several GeV on atomic nuclei are a subject of great interest for over a half of a century, the mechanism of these reactions is still not understood satisfactorily. Reactions caused by protons at intermediate and high energies with such preactinide nuclei as Bi, Ta, W, Au, have been studied in a number of works [1–7] using different methods and techniques, where special attention has been put on the fission and/or spallation phenomena. It has been observed, that the increase of the proton-beam energy from a value, comparable with the Fermi motion energy of nucleons in nuclei, to several GeV leads to a fast increase of the cross sections for the production of reaction fragments—even by one order of magnitude. However, satisfactorily, the quantitative description of the data is still lacking. The data obtained in these works, the subsequent analysis of the results, and the comparison with available model calculations allowed one to reproduce the cross section behavior as well as to come to the important conclusions about the reaction mechanisms. In this context, nuclear data, being the quantitative characteristics of nuclear reactions, have become important in the intermediate and high energy range. They are important for the development of new concepts of nuclear energy production and changing of radioactive waste.

The theoretical model calculations represent an additional source of cross section data and other important reaction characteristics. Frequently, many approaches discussed in the literature and assuming various reaction mechanisms are able to reproduce the observed phenomena only partially. Even the total production cross sections and their energy variation can be, at present, predicted by the theory with moderate success only, i.e., deviations of the theoretical cross sections from data are frequently larger than a factor of two. Besides the obvious need to understand the mechanism of proton-induced reactions, there is also a broad range of applications which must rely on model predictions of the cross sections of such reactions. For example, the reliable data for the design and construction of spallation neutron sources and/or accelerator driven systems must be known for various proton-beam energies on many targets and for different reaction products. The number of different reactions important for such applications is so large, that it is practically impossible to determine all these cross sections experimentally. On the contrary, knowledge of reaction mechanisms should allow for the creation of realistic theoretical models, which are able to provide cross sections for all interesting reactions—even those which cannot be studied experimentally. It is, therefore, clear that studying of the mechanism of proton-induced reactions is crucial both for fundamental physical studies and for the applications. However, the experimental data are not sufficient, especially in the case of the $^{209}$Bi target, due to the limited number of facilities available, and more data are still required for benchmarking calculations and for the adjustment of model parameters. Among the different preactinide targets, the $^{209}$Bi target is less studied experimentally, so a survey on the literature displays that there is a considerable lack of experimental data, in particular, for the proton-induced reaction. The detailed investigation of the main properties of the reaction will allow tracking the evolution of the main

 

characteristics of the different reaction channels from the light target to heavy ones.

During recent years we have investigated systematically the production of the residual nuclides induced by high-energy protons and deuterons [8–11]. The main goal of these studies was to find the difference or the similarity of the main features between the collision of protons and deuterons at the same total kinetic energy of the projectile as well as to provide a database for model calculations by exclusive and new results. The current paper, devoted to the study of the 660 MeV proton-induced reaction on a $^{209}$Bi target, will continue the series of experiments by using the proton beam as a projectile. In experiments on such heavy actinide targets as $^{237}$Np, $^{238}$U, $^{241}$Am [12–14], a decomposition of the fission mass-yield distribution allowed to separate the different fission modes. Using a preactinide nucleus as a target gives us a new opportunity to understand the reaction mechanism, as well as to observe the transition of the main properties of a highly excited nucleus from the intermediate to heavy range of masses and from intermediate- to high-energy projectiles.

The goal of the present study is to measure the reaction product cross section for a $^{209}$Bi nucleus in an extracted beam of protons from the phasotron of the Laboratory of Nuclear Problems at the Joint Institute of Nuclear Research (JINR, Dubna) at 660 MeV. The obtained experimental data allowed to estimate the contribution of the different reaction channels such as fission and spallation and compare with experimental data from [1] at approximately the same incident energy of the proton beam as well as with theoretical model calculations using the CRISP code.

## II. EXPERIMENTAL PROCEDURE

A pure $^{209}$Bi target, having a natural isotopic composition, was prepared in the form of four stacked foils in the form of discs of diameter 1.4 cm each. The target was exposed to an accelerated proton beam of 660 MeV from the phasotron of the Laboratory of Nuclear Problems at the Joint Institute of Nuclear Research (JINR, Dubna). The irradiation time was 5.3 h at proton-beam intensity of $1.67 \times 10^9$ particles per second. The total weight of the target was 2.55 g and a total thickness of 600 $\mu$m. Each target was sandwiched by a pair of 50 $\mu$m Al foils with the same size. All foils were piled up together and aligned perpendicularly to the beam direction. The reaction $^{27}$Al$(p, 3pn)^{24}$Na with cross sections of 10.2 mb [15] for beam monitoring was used. The measurements of the spectra of $\gamma$ rays emitted during the decays of radioactive reaction products began 2 h after the completion of the irradiation and lasted five months by using four HpGe detectors with energy resolution 0.23% at an energy of 1332 keV. The energy-dependent detection efficiency of the HpGe was measured with standard calibration sources of $^{54}$Mn, $^{57;60}$Co, $^{137}$Cs, $^{154}$Eu, $^{152}$Eu, and $^{133}$Ba. The half-lives of identified isotopes were within the range of 15 min and 1 yr. The error in determining cross sections depended on the following factors: the statistical significance of experimental results ($\leqslant$2–3%), the accuracy in measuring the target thickness and the accuracy of tabular data on nuclear constants ($\leqslant$3%), and the errors in determining the detector efficiency with allowance for the accuracy in calculating its energy dependence ($\leqslant$10%). Nuclear properties, used for identification of observed isotopes as nuclear transition energies, intensities, and half-lives were taken from literature [16].

The independent production of a reaction product nuclide ($I$), i.e., the cross section for the nuclide to be made directly in the reaction in the absence of a parent isotope (which may give a contribution in measured cross section via $\beta^{\pm}$ decays) can be determined by using the following equation:

$$\sigma = \frac{\Delta N\ \lambda}{N_p N_n k \epsilon \eta (1 - \exp(-\lambda t_1)) \exp(-\lambda t_2)(1 - \exp(-\lambda t_3))}, \tag{1}$$

where $\sigma$ is the cross section of the reaction fragment production (mb); $\Delta N$ is the area under the photopeak; $N_p$ is the proton–beam intensity (min$^{-1}$); $N_n$ is the number of target nuclei (in 1/cm$^2$ units); $t_1$ is the irradiation time; $t_2$ is the time of exposure between the end of the irradiation and the beginning of the measurement; $t_3$ is the measurement time; $\lambda$ is the decay constant (min$^{-1}$); $\eta$ is the relative intensity of $\gamma$ transitions; $k$ is the total coefficient of $\gamma$-ray absorption in target and detector materials, and $\epsilon$ is the $\gamma$-ray detection efficiency.

In the case of cumulative production cross section ($C$), when a given isotope is made in all the appropriate processes, i.e., both directly in the reaction and over time due to the decays of all of its chain precursors, the cross section calculation becomes more complicated [17]. If the formation cross section of the parent isotope is known from experimental data, or if it can be estimated on the basis of other sources, the independent cross sections of daughter nuclei can be calculated by the relation

$$\begin{aligned}\sigma_B = & \frac{\lambda_B}{(1 - \exp(-\lambda_B t_1))\ \exp(-\lambda_B t_2)(\,1 - \exp(-\lambda_B t_3))} \\ & \times \left[ \frac{\Delta N}{N_p\, N_n\, k\, \epsilon\, \eta} - \sigma_A\, f_{AB}\, \frac{\lambda_A\, \lambda_B}{\lambda_B - \lambda_A} \right. \\ & \times \left( \frac{(1 - \exp(-\lambda_A t_1))\ \exp(-\lambda_A t_2)\,(1 - \exp(-\lambda_A t_3))}{\lambda_A^2} \right. \\ & \left. \left. - \frac{(1 - \exp(-\lambda_B t_1))\ \exp(-\lambda_B t_2)\,(1 - \exp(-\lambda_B t_3))}{\lambda_B^2} \right) \right],\end{aligned} \tag{2}$$

where the subscripts $A$ and $B$ label variables referring to, respectively, the parent and the daughter nucleus; the coefficient $f_{AB}$ specifies the fraction of $A$ nuclei decaying to a $B$ nucleus ($f_{AB} = 1$, when the contribution from the $\beta$ decay corresponds 100%); and $(\Delta N)_{AB}$ is the total photopeak area associated with the decays of the daughter and parent isotopes. The effect of the precursor can be negligible in some limiting cases: where the half-life of the parent nucleus is very long, or in the case where its contribution is very small. It should be mentioned that the use of the induced-activity method imposes several restrictions on the registration of the reaction products. For example, it is impossible to measure a stable and very short-lived, very long-lived isotopes.

TABLE I. The cross sections of nuclides formed by the reaction of 660 MeV protons with $^{209}$Bi. Independent cross sections are indicated by (I); others are cumulative (C).

| Nuclide | Type | $\sigma$, mb | Nuclide | Type | $\sigma$, mb |
|---|---|---|---|---|---|
| $^{24}$Na | C | 0.17 ± 0.04 | $^{110m}$Ag | I | 3.29 ± 0.60 |
| $^{28}$Mg | C | 1.05 ± 0.11 | $^{113}$Sn | C | 1.10 ± 0.15 |
| $^{42}$K | C | 0.08 ± 0.01 | $^{118m}$Sb | I | 1.43 ± 0.23 |
| $^{46}$Sc | I | 0.20 ± 0.04 | $^{119}$Te | C | 0.73 ± 0.06 |
| $^{47}$Ca | C | 0.28 ± 0.05 | $^{119m}$Te | C | 0.66 ± 0.04 |
| $^{52}$Mn | C | 0.54 ± 0.08 | $^{120m}$Sb | I | 1.04 ± 0.22 |
| $^{56}$Co | C | 0.33 ± 0.06 | $^{121}$Te | C | 1.71 ± 0.18 |
| $^{57}$Ni | C | 2.47 ± 0.24 | $^{121m}$Te | C | 0.76 ± 0.15 |
| $^{59}$Fe | C | 1.08 ± 0.22 | $^{124}$Sb | I | 0.82 ± 0.15 |
| $^{65}$Zn | C | 0.95 ± 0.07 | $^{127}$Sb | C | 1.12 ± 0.27 |
| $^{66}$Ga | C | 0.92 ± 0.07 | $^{127}$Xe | C | 1.51 ± 0.18 |
| $^{69}$Ge | C | 1.15 ± 0.23 | $^{131m}$Te | C | 2.18 ± 0.45 |
| $^{72}$Zn | C | 0.41 ± 0.17 | $^{140}$La | C | 0.48 ± 0.04 |
| $^{72}$Ga | I | 1.93 ± 0.19 | $^{148m}$Pm | I | 0.11 ± 0.02 |
| $^{74}$As | I | 3.03 ± 0.13 | $^{154}$Tb | I | 0.05 ± 0.01 |
| $^{75}$Se | C | 1.46 ± 0.61 | $^{169}$Lu | C | 2.73 ± 0.58 |
| $^{76}$Br | C | 3.63 ± 0.64 | $^{170}$Lu | C | 5.54 ± 1.05 |
| $^{88}$Y | C | 5.47 ± 0.40 | $^{172}$Lu | C | 3.80 ± 0.41 |
| $^{89}$Zr | C | 2.94 ± 0.60 | $^{175}$Ta | C | 11.17 ± 2.00 |
| $^{90}$Nb | C | 1.31 ± 0.16 | $^{185}$Ir | C | 23.90 ± 2.58 |
| $^{93m}$Mo | C | 2.05 ± 0.40 | $^{194}$Au | I | 3.33 ± 0.36 |
| $^{96}$Nb | I | 4.36 ± 1.11 | $^{203}$Bi | C | 30.75 ± 3.71 |
| $^{96}$Tc | I | 2.03 ± 0.41 | $^{205}$Bi | C | 54.83 ± 5.36 |
| $^{100}$Rh | C | 4.15 ± 0.80 | $^{206}$Bi | C | 31.23 ± 6.49 |
| $^{106m}$Ag | I | 1.79 ±0.27 | – | – | – |

The main limitation of this technique is that neither short-lived nor stable residual nuclei can be measured.

## III. RESULTS AND DISCUSSION

The experimental cross sections of the reaction fragments in the mass range of $24 \leqslant A \leqslant 210$ u formed from 660 MeV protons interacting with $^{209}$Bi were measured and presented in Table I and Fig. 1.

In order to obtain a complete picture of the charge and mass distributions of the reaction products, it is necessary to estimate the cross sections of isotopes unmeasurable by the induced activity method. The isobaric yield distribution depicts the variation of independent yield with an atomic number of the isobar for a given mass number. Such variation can usually be expressed as a Gaussian distribution function [18]:

$$\sigma(A,Z) = \frac{\sigma(A)}{(C\pi)^{1/2}} \exp\left(-\frac{(Z-Z_p)^2}{C}\right), \tag{3}$$

where $\sigma(A,Z)$ is the independent cross section for a given nuclide with an atomic charge $Z$ and a mass number $A$, $\sigma(A)$ is the total isobaric cross section of the mass chain $A$, $Z_p$ is the most probable charge for that isobar, and $C$ is the width parameter of the distribution for the mass number $A$. Parameters of charge distribution determine the position of residue nucleus concerning the isotopes with maximum yield in an isobaric chain. In the assumption of the constant

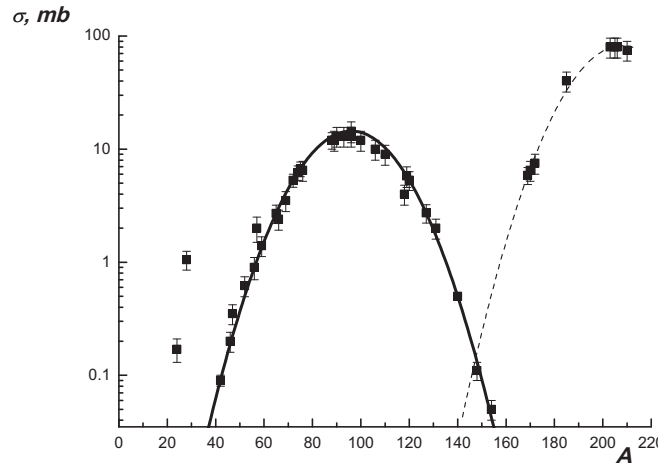


FIG. 1. Mass-yield distribution for the interaction of 660 MeV proton-induced reaction on a $^{209}$Bi target. The black continuous curve corresponds to the fission cross section, the dashed indicates the spallation cross section, and experimental data are represented by the solid squares.

width parameter of charge distributions for different mass chains [18], the least-squares method was applied in order to get fitting parameters $Z_p$ and $\sigma(A)$. The cross section of a particular isotope $(Z, A)$ may be independent, partly, or completely cumulative depending on decay chains of precursors. During the fitting procedure, the experimental cumulative cross section was then corrected for precursors contribution.

The calculated values of $\sigma(A)$ that correspond to the total isobaric cross sections of the reaction fragments for a specific mass number $A$, made it possible to construct the mass-yield distribution. The mass-yield distributions of fission fragments were analyzed on the basis of symmetric mass distribution in the following form [7]:

$$\sigma_f(A) = \lambda_A \exp\left(-\frac{(A-M_A)^2}{\Gamma_A^2}\right). \tag{4}$$

Gaussian curve (4) represents the symmetric mass distribution defined by a height $\lambda_A$, a mean mass $M_A$, and a width $\Gamma_A$. Integrating over the Gaussian and multiplying with a factor 0.5, because of the two fission fragments in each fission event, gives an estimation for the fission cross section. In Fig. 1 the mass-yield distribution, obtained by the fitting procedure, is represented by the solid curve. The values of the fit parameters together with the fission cross section are tabulated in Table II. Analysis of the mass distribution curve made it possible to determine the positions of a peak, the width of mass distribution as well as the total amount of the total number of

TABLE II. Fitted values of the parameters in Eq. (4) and fission cross section $\sigma_f$.

| | |
|---|---|
| $\Gamma_A$ | 24.0 ± 0.3 |
| $\lambda_A$ | 13.1 ± 0.5 |
| $M_A$ | 96.0 ± 0.2 |
| $\sigma_f$ (mb) | 279.0 ± 56.0 |

emitted neutrons from the hot composite system, $\nu_T$. From the mean value of the mass distribution, it can be concluded that on the average 18 neutrons are emitted before and after fission, since the mass distribution peak has a maximum of about $A \approx 96$ u. Presumably, a nucleus undergoes symmetric fission at an average mass-number value of $A_f \approx 192$ u.

The fission cross section induced by protons of the present work is in good agreement with the phenomenological systematics and parametrizations, performed by the compilation of proton-induced fission cross section data for targets from $^{165}$Ho to $^{239}$Pu at the same excitation energy [19].

As is seen from Fig. 1, there is a large hump consisting of the heavy residues in the mass range below the corresponding target mass that can be observed. The processes connected to the production of such nuclei would be spallation or deep spallation. The region of isobars with masses $A < 40$ u would correspond to the intermediate mass fragments (IMFs). The group of the fragments is this mass region cannot be unequivocally identified. One of the possible mechanisms for the production of IMFs is that they would correspond to the counterpart pair of products in the mass region $A \approx 140$–$160$ u. It means that they could originate from a deep spallation process in which nuclides would emit not only nucleons and light charged particles (with $Z \leqslant 2$) but also some heavier elements in the IMF region. Moreover, an alternative explanation of the origin of IMF products was suggested by the intranuclear cascade model [20], according to which these fragments are the result of the disintegration of the excited residual nucleus with masses near the target mass after evaporation of the nucleons.

In Ref. [21] the semiempirical approach estimation of the fission probability prediction of neutron-, proton-, and photon-induced fission reactions in the intermediate energy region from several tens of MeV to 3 GeV has been done. According to above-mentioned systematization, the fissility for bismuth isotopes increases with excitation energy at around 100 MeV to a value of 6% and reaches saturation at 200 MeV with a value of 14–15%. The fissility ($D$) is defined by the ratio $\sigma_f/\sigma_{\text{in}}$, where $\sigma_f$ is the fission cross section and $\sigma_{\text{in}}$ is the total inelastic cross section. Also, fissility is an nondimensional quantity.

For the fission process studied in the present paper, we deduced the value $\sigma_{\text{in}} = 1975 \pm 395$ mb, which was obtained by summing the cross sections for all channels of the reaction (fission, spallation-evaporation, and IMFs production). The fissility of fissioning nuclei in this work is consistent to nucleon-induced fission reactions at intermediate energies [21] and reaches the value of $0.14 \pm 0.03$. The fissility, $D$, as a function of the fissility parameter, $Z^2/A$, for the fissile system of the present work together with the experimental data obtained earlier using $^{241}$Am, $^{238}$U, and $^{237}$Np targets at the same incident energy [12,13] are presented in Fig. 2. As can be noticed, the fissility is a smooth function of $Z^2/A$. It increases monotonically from the value for the Bi target up to the value for Am target but still remains below unity, reaching saturation, since nuclei with high $Z^2/A$ may follow other decay channels besides fission such as nucleon evaporation with production of spallation residues although with lower chance.

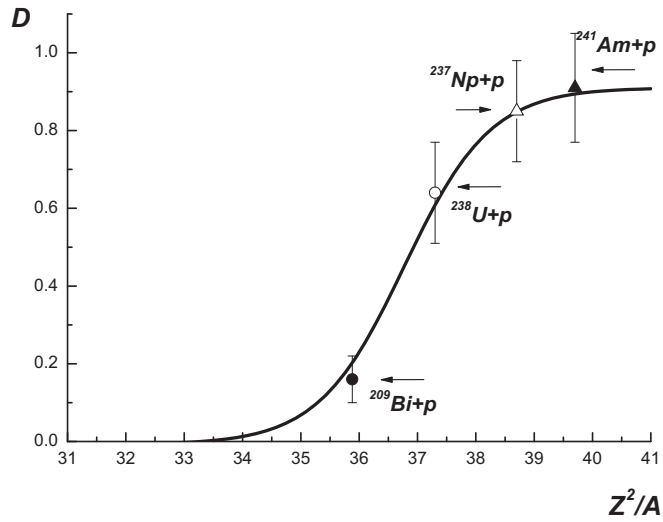


FIG. 2. Fissility $D$ as a function of $Z^2/A$ of the fissile system. Presented symbols for the experimental data are $p + ^{241}$Am (▲), $p + ^{237}$Np (○) [12], $p + ^{238}$U (△) [13], and $p + ^{209}$Bi (●) (present work). The solid line is displayed as a guide.

The analysis of both the neutron emission and the contribution of symmetric fission relative to total fission cross section ($\sigma_{\text{sym}}/\sigma_f$) in the case of four targets under study, $^{209}$Bi (present work), $^{241}$Am, $^{238}$U, and $^{237}$Np (Refs. [12,13]) at the same proton incident energy allows to suggest that the total number of emitted neutrons ($\nu_T$) is directly proportional to the symmetric fission contribution. This correlation can be visualized on Fig. 3. From the obtained data it follows that the fission of preactinide $^{209}$Bi nucleus is totally symmetric, while in the case of the other targets studied in previous works,

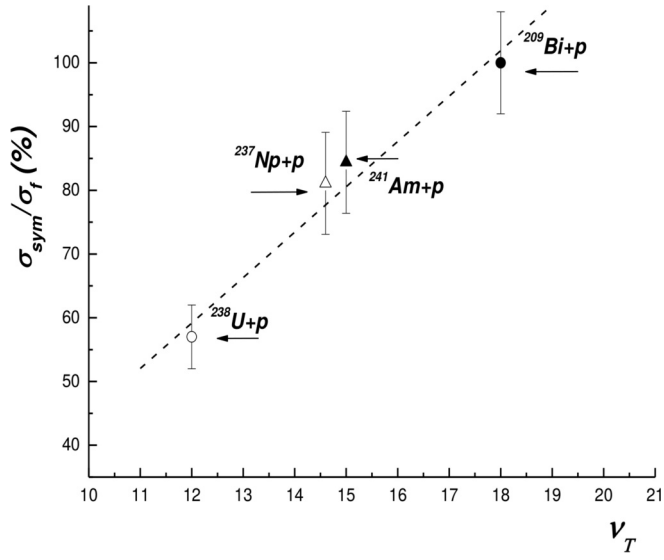


FIG. 3. Contribution of the symmetric fission to the total fission cross section ($\sigma_{\text{sym}}/\sigma_f$) as a function of the total number of emitted neutrons ($\nu_T$). Presented symbols for experimental data are $p + ^{241}$Am (▲) [12], $p + ^{238}$U (△) [13], $p + ^{237}$Np (○) [12], and $p + ^{209}$Bi (●) (present work). The dashed line is displayed as a guide.

TABLE III. The average and critical fissility parameters of the fissioning nuclei at 660 MeV of proton energy for $^{241}$Am, $^{238}$U, $^{237}$Np (Refs. [12,13]), and $^{209}$Bi (present work) targets.

| Target | $^{241}$Am | $^{238}$U | $^{237}$Np | $^{209}$Bi |
|---|---|---|---|---|
| $(Z^2/A)_{\text{cr.}}$ | 37.5 | 36.3 | 36.7 | 32.7 |
| $Z^2/A$ | 39.7 | 37.3 | 38.7 | 35.9 |

the asymmetric fission contributes, to a lower or a higher degree, to the total fission cross section. The presence of an asymmetric fission component in the energy region under consideration for $^{241}$Am, $^{238}$U, and $^{237}$Np requires a brief explanation. It may be a consequence of a large spread of the excitation energies of the fissioning systems. These systems come from different chains of nucleonic evaporation which begin right after the primary interaction with the projectile and goes on up to the moment of fission. Different fissioning systems end up with different sets of mass number, charge, and excitation energy, the latter being low in some cases and high in other. The population of the fissioning system with low excitation energies provides the asymmetric fission contribution that is observed in the final mass distribution of fragments while the high excitation energy population provides the symmetric contribution. Finally, as is well known, an increase in the excitation energy contributes to the symmetric decay of the nucleus [22], whereas low-energy fission is basically asymmetrical in nature. Alongside this, a higher excitation energy is coupled to an increase in neutron evaporation, therefore the correlation observed in Fig. 3. According to the previous work in Ref. [12], the asymmetric component indeed manifests itself stronger in the case of the $^{238}$U target and Fig. 3 shows that the number of neutrons emitted for the $^{238}$U target is the lowest among the reactions studied. As a final statement, the increase in neutron evaporation results in a larger contribution of the neutron-deficit nuclides with higher fissility parameter.

The systematization of cross sections for symmetric and asymmetric fission in a wide range of nuclei carried out in [23] showed that it is possible to use an empirical expression for estimating the probability of the different fission modes. In order to characterize this factor quantitatively, the authors introduced a critical value of the fissility parameter, in the form

$$(Z^2/A)_{\text{cr.}} = 35.5 + 0.4(Z_f - 90), \tag{5}$$

where $Z_f$ is the charge of the fissioning nucleus. According to [23], for the nuclei with $Z^2/A$ values greater than the critical value, the symmetric fission mode was dominant, but, at smaller values of the fissility parameter, the main fission channel leads to asymmetric fragments. The average and critical fissility parameters of the fissioning nuclei at low and high incident energies for $^{241}$Am, $^{238}$U, $^{237}$Np (Refs. [12,13]), and $^{209}$Bi (present work) are tabulated in Table III. From Table III one can see that the difference between the mean and the critical fissility parameters for $^{238}$U, $^{237}$Np, $^{241}$Am, and $^{209}$Bi targets is increased and equals, correspondingly, to 1.0, 2.0, 2.2, and 3.2, which is clearly seen in Fig. 3.

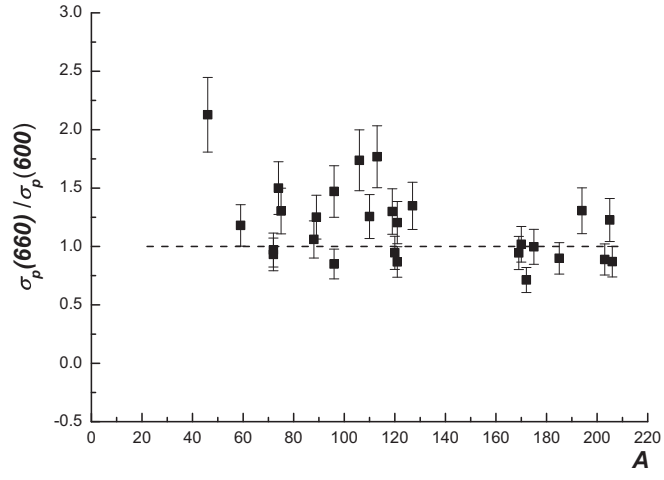


FIG. 4. Cross section ratios, $\sigma_p(660)/\sigma_p(600)$, of residues from 660 and 600 MeV proton-induced reactions of present work and from Ref. [1].

During the interaction with protons, the energy transferred to the heavy nucleus is redistributed among the nucleons of the composite system. In this regard it is interesting to see the effect of an increased excitation energy of the composite nucleus. This can be done by comparing the data of the present paper with the data from the reaction with the same target and projectile but at a lower incident energy. In Fig. 4, we show a comparison between fragment cross sections for the same fragments in two different studies, the reaction of the present study, $^{209}$Bi + 660 MeV $p$, where $p$ stands for proton, and the reaction $^{209}$Bi + 600 MeV $p$ [1]. The cross sections from these studies are represented in Fig. 4 by $\sigma_p(660)$ and $\sigma_p(600)$, respectively, where $p$ stands for proton once again. The points represent the ratios of individual cross sections. In Fig. 4 one can see two mass regions corresponding to the fragment formation cross section during the fission and spallation-evaporation processes. The points represent the ratios of individual cross sections. As one can see in Fig. 4, that the cross sections for the heavy mass fragments with $A >$ 160 (fragments formed in the spallation-evaporation process) are almost the same as those for proton-induced reactions at 660 MeV. Namely, the ratios of the cross section ratio for this mass range is $0.98 \pm 0.15$. As it was shown in our previous papers [8,9], these nuclides are formed in a peripheral collision with a large impact parameter and low excitation energy. In the mass range $55 \leqslant A \leqslant 130$, where one can expect the huge contribution of fission fragment production, the ration of the cross sections, on average, is higher for the energy 660 MeV of the present study. The cross section ratio for this mass range is $1.49 \pm 0.22$. The enhanced cross section of such mass range in the proton-induced reaction can be interpreted in terms of changing the reaction mechanism. These reaction products are produced in more central collisions [8,9], with lower impact parameters, and are responsible for the formation of high-excitation remnants. There is only one fragment, $^{46}$Sc, with the cross section value somewhat higher than other fission production cross sections. One can explain this fact by the growing contribution of the IMF production which is more pronounced at 660 MeV.

## IV. CRISP CALCULATION

The CRISP program has been used to calculate the reaction $^{209}$Bi + 660 MeV protons from the first interaction to fragments production. Details of the relevant models used by CRISP and the discussion of the results are presented in the following.

### A. Model description

The CRISP model (acronym for Collaboration Rio - Ilhéus - São Paulo) calculates nuclear reactions [24] in a two step process. The intranuclear cascade is the first step. It begins after a primary interaction with an incident particle [25–28]. The proton can interact elastically or inelastically producing resonances ranging from the $\Delta_{1232}$ to $N^*_{2250}$. Double resonance production is also possible. A photon can interact according to the channels that go from the quasideuteron absorption mechanism at around 50 MeV up to hadronization and vector meson production [29–31]. The most relevant nucleonic resonances at intermediate energy are also produced.

Secondary particles, created during the cascade, may interact with other particles or reach the surface of the nucleus which is constructed as a Fermi gas. Nucleons with kinetic energy above the nuclear potential may leave, otherwise they are reflected. The tunneling of protons through the Coulomb potential is also considered. The multicollisional approach allows a more realistic simulation of the intranuclear cascade [24]. Since all particles move simultaneously, the order of events is established by the time sequence between collisions of each pair of particles and respective cross sections. Such an approach makes it natural to verify dynamical aspects, e.g., nuclear density modification and level occupation evolution of the gas.

The Pauli blocking mechanism is another important feature in the model. Once all nucleons are located in Fermi gas levels and they are allowed to move simultaneously, exchanging energy and momentum, the exclusion principle can be verified strictly [24].

At the intranuclear cascade stage, CRISP is a multicollisional model, meaning that all nucleons inside the nucleus have their position modified according to their initial position and their momenta. In this aspect, only CRISP and the Liege [32] models follow such realistic calculations of the intranuclear cascade. This novelty allows a more reliable calculation of the fast stage of nuclear reactions, since it naturally takes into account the fast modifications of the nuclear density while the intranuclear cascade evolves. Another aspect that is improved by introducing the multicollisional method is the possibility to calculate the effects of the Pauli principle, which blocks part of the process at energies near the Fermi energy. In CRISP we use a strict calculation of the Pauli blocking mechanism, which leads to more precise results. In fact, even if the incident particle energy is high, at some point the Pauli blocking mechanism becomes important, and the larger the number of particles participating in the intranuclear cascade, the more important the blocking mechanism is to correctly calculate energy, mass number, and atomic number distributions at the end of the intranuclear cascade. Old Monte Carlo models, which do not present the multicollisional method, may still give good results for cross sections, since modifications of the intranuclear cascade due to nuclear density modifications and due to Pauli blocking can be calculated by simple models, however, more parameters must be introduced and must be fitted to experimental data in order to give good results. Therefore, CRISP and the Liege models are the most reliable models to be used when no experimental data are available, or to investigate aspects of the nuclear reaction that cannot or are difficult to be observed experimentally.

Also another feature that is made possible by the multicollisional approach is the energetic stop criterion since the particle's kinetic energy is reliable information in this approach. When no particle has kinetic energy above the potential, mass and atomic number and excitation energy can no longer change, the nucleus is considered thermalized and the cascade is ended since the next step regarding the competition between fission and evaporation of particles is calculated only statistically.

In this second stage, the emission widths are determined according to Weisskopf's model [33] and calculated relative to the neutron emission width as

$$\frac{\Gamma_p}{\Gamma_n} = \frac{E_p}{E_n} \exp\{2[(a_p E_p)^{1/2} - (a_n E_n)^{1/2}]\}, \tag{6}$$

for proton emission and

$$\frac{\Gamma_\alpha}{\Gamma_n} = \frac{2E_\alpha}{E_n} \exp\{2[(a_\alpha E_\alpha)^{1/2} - (a_n E_n)^{1/2}]\}, \tag{7}$$

for $\alpha$ particles emission. The energies of the possible final states are given by

$$\begin{aligned} E_n &= E - B_n, \\ E_p &= E - B_p - V_p, \\ E_\alpha &= E - B_\alpha - V_\alpha, \end{aligned} \tag{8}$$

where $E$ is the current energy of the nucleus. $B_n$, $B_p$, and $B_\alpha$ are the separation energies for neutrons, protons, and $\alpha$ particles, respectively. The separation energies are calculated using the semiempirical mass formula from Pearson [34]. $V_p$ and $V_\alpha$ are the Coulomb potentials for protons and $\alpha$ particles.

The level density parameters $a_n$, $a_p$, and $a_\alpha$ for neutrons, protons, and $\alpha$ particles are determined by Dostrovsky's equations [35].

The fission process follows the Bohr and Wheeler model [36] with the fission width calculated according to Vandenbosch and Huizenga [37]:

$$\frac{\Gamma_f}{\Gamma_n} = K_\mathrm{f} \exp\{2[(a_f E_f)^{1/2} - (a_n E_n)^{1/2}]\} \tag{9}$$

with

$$K_f = K_0 a_n \frac{[2(a_f E_f)^{1/2} - 1]}{(4A^{2/3} a_f E_n)} \tag{10}$$

and

$$\begin{aligned} E_f &= E - B_f, \\ a_f &= r_f a_n, \end{aligned} \tag{11}$$

where $B_f$ is the fission barrier calculated according to Nix model [38]. $a_f$ is the fission level density parameter with $r_f$ being a adjustable parameter.

In the CRISP model, the hot nucleus evaporates until either the excitation energy becomes smaller than the neutron separation energy or until fission occurs, which may happen at any point of the evaporation chain. In the case of fission, the CRISP model determines the masses of the fission fragments according to the multimodal fission model, best known in the literature as the random neck rupture model [39,40]. The total yield of the fragment mass distribution is the incoherent sum of the contributions of all fission modes, each one being described by a Gaussian mass distribution positioned at the most probable mass for the fragment. The superlong mode (SL) represents symmetric fission. Thus, it requires only one Gaussian. The standard 1 (S1) and 2 (S2) modes describe asymmetric fission for low and intermediate nuclear deformation, respectively. The standard 3 (S3) mode describes superasymmetric fission, i.e., fission of highly deformed systems. Each asymmetric mode requires two Gaussian distributions, one centered at the heavy and the other centered at the light fragment most probable mass. The charge distribution is also Gaussian.

The total yield for a fragment with mass number A and atomic number Z is determined by

$$\sigma(A,Z) = \left\{ \sum_i \left[ \frac{K_i}{\sqrt{2\pi}\Gamma_i} \exp\left( -\frac{\left(A - A_i^{\mathrm{L}}\right)^2}{2(\Gamma_i)^2} \right) + \frac{K_i}{\sqrt{2\pi}\Gamma_i} \exp\left( -\frac{\left(A - A_i^{\mathrm{H}}\right)^2}{2(\Gamma_i)^2} \right) \right] + \frac{K_{\mathrm{SL}}}{\sqrt{2\pi}\Gamma_{\mathrm{SL}}} \exp\left( -\frac{(A - A_{\mathrm{SL}})^2}{2(\Gamma_{\mathrm{SL}})^2} \right) \right\} \times \frac{1}{\sqrt{2\pi}\Gamma_Z} \exp\left( -\frac{(Z - \overline{Z_0})^2}{2\Gamma_Z^2} \right), \quad (12)$$

where the summation runs over the asymmetric modes. The parameters for the symmetric mode are $K_{\mathrm{SL}}$, $A_{\mathrm{SL}}$, and $\Gamma_{\mathrm{SL}}$, while $K_i$ and $\Gamma_i$ are the parameters for the fragments produced in the asymmetric mode $i = \mathrm{S1}, \mathrm{S2}, \mathrm{S3}$. The position parameters $A_i^{\mathrm{H(L)}}$ for the heavy (light) fragments are determined as $A_i^{\mathrm{H}} = A_{\mathrm{SL}} + D_i$ and $A_i^{\mathrm{L}} = A_{\mathrm{SL}} - D_i$. The shift $D_i$ is the adjustable parameter. The positions of the Gaussians, the widths are parameters only determined through comparison to the total experimental mass distribution. CRISP is able to calculate total fission and spallation cross sections.

It is important to mention that the parameters $K_i$ and $K_{\mathrm{SL}}$ represent the probability of the respective fission modes, not cross sections since the Brosa model is applied in CRISP by means of a Monte Carlo method.

According to the Monte Carlo method applied in this model, each simulated fission history leads to a particular fissioning system with a particular $A_{\mathrm{SL}}$. This variation of $A_{\mathrm{SL}}$ is considered by the CRISP model in Eq. (12) making the choice of the fragments unique and folding together the fissioning system mass distribution and the fragment mass distribution, what is quite in accordance with reality.

For the atomic number distribution the parametrization used is [18]

$$\overline{Z_0} = \mu_1 + \mu_2 A \quad (13)$$

for the most probable atomic number of the fragment, and

$$\Gamma_Z = \nu_1 + \nu_2 A \quad (14)$$

for the width of the atomic number distribution. $\mu_1$, $\mu_2$, $\nu_1$, and $\nu_2$ are fitting parameters.

The fissioning system excitation energy is divided between the fragments following a mass proportion, i.e.:

$$E^*_{\mathrm{frag1}} = \frac{A_{\mathrm{frag1}}}{A_f} E^*_f, \quad (15)$$

$$E^*_{\mathrm{frag2}} = \frac{A_{\mathrm{frag2}}}{A_f} E^*_f, \quad (16)$$

where $E^*$ are excitation energies and $A_f$ is the mass of the fissioning system.

After determination of the fission fragments they are allowed to evaporate following the already mentioned statistical evaporation model of Weisskopf. The final products of fission can then be compared to experimental data.

### B. Calculation results and discussion

Concerning the production of fission fragments for the reaction studied, only the symmetric fission channel was considered, since the experimental analysis shows no evidence of asymmetric fission channels. This means that the parameter $K_{\mathrm{SL}}$ in Eq. (12) represents alone a probability of 100%. For the width of fission fragment mass distribution before fragments evaporation, parameter $\Gamma_{\mathrm{SL}}$, the value of 17 was imposed. The final width of the mass yield may be different not only because the fragments evaporate but mostly because the evaporation rate is different between heavier and lighter fragments. The spallation residues are obtained directly from the chain of evaporation calculated using Weisskopf's model [33], as mentioned in Sec. IV A. Table IV shows fission and spallation cross sections along with relevant results obtained for the fission mass-yield distribution.

The results obtained by CRISP are totally consistent with those obtained by the fitting procedure. One can see from Table IV that the evaporation of the fragments indeed changed

TABLE IV. Fission and spallation cross sections along with relevant results obtained for the fission mass-yield distribution.

| | |
|---|---|
| Total fission cross section - $\sigma_f$ (mb) | $217 \pm 1$ |
| Total spallation cross section - $\sigma_s$ (mb) | $1799 \pm 1$ |
| Average fissioning system mass | 199 |
| Average fission fragment mass (after fragments evaporation) | 95 |
| Width of fission fragment mass distribution (before fragments evaporation) | 17 |
| Width of fission fragment mass distribution (after fragments evaporation) | 16.8 |
| $(Z^2/A)_{\mathrm{cr.}}$ | 32.22 |
| $Z^2/A$ | 33.17 |

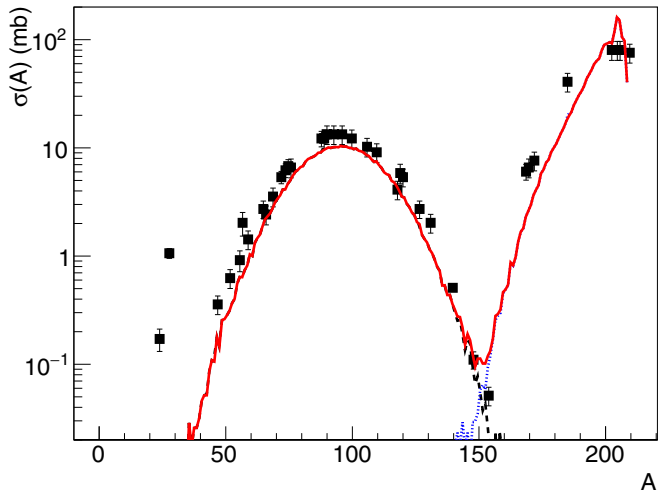


FIG. 5. Calculated fission and spallation mass-yield distribution for the interaction of 660 MeV proton-induced reaction on a $^{209}$Bi target. Black dashed line represents the fission mass yield while the blue dotted line represents the spallation mass yield. The solid red line stands for the total mass yield.

the width of fission fragment mass distribution although not appreciably. In this case in particular, the heavier fragments had a higher evaporation rate. This can be explained by the bigger share of the fissioning system's excitation energy that goes to the heavier fragment.

The evaporation-fission competition calculated by CRISP also provided the distribution of fissioning systems. From that we obtained an average atomic number of 81.8 which leads to a critical fissility parameter of 32.22. This value is very close to the one estimated at Sec. III. By calculating the entire chain of evaporation to the fission point, CRISP can also determine the fissility parameter observed for all fissioning systems. The average fissility parameter was found to be 33.17. Although this value is lower than the one estimated in the Sec. III estimation, and the CRISP simulation is in qualitative agreement and just as estimated the symmetric fission mode alone was enough for CRISP to achieve a good reproduction of the data. Both critical and average fissility parameter can also be seen in Table IV.

Figure 5 shows the total mass-yield calculated by CRISP in comparison to the experimental data. The mass yields from fission and spallation separately are also shown. The result is considered good in general and particularly good for the fission part. For the spallation residues, the issue that stands out is the overestimation of the cross sections of some high-mass fragments at the cost of the low-mass fragments. This is a clear indication that CRISP is finishing the chain of evaporation too soon. Despite that, it is possible to argue that the total spallation cross section is in good agreement with the measured data. The overestimation occurs only for the already high cross sections at around mass 200. An adequate fixing at this point would almost entirely compensate for the underestimation observed for the rest of the curve which lies in regions of lower cross sections.

## V. CONCLUSION

The present measurements were carried out in order to provide the analysis charge and mass of the proton-induced reaction products on a $^{209}$Bi target at 660 MeV. The total isobaric yields of the different mass chains of the reaction fragments were estimated assuming a Gaussian charge distribution with the constant width parameter $C$. The mass-yield distribution of the fission fragments was estimated by integrating over the Gaussian in the suggestion of the symmetric fission channel. The value of the obtained fission cross section, determined by summing over all mass fragments, was equal to $279.0 \pm 56.0$ mb. The fissility of the fissioning nucleus at intermediate energy was estimated at $0.14 \pm 0.03$.

## ACKNOWLEDGMENTS

G.K. thanks FAPESP (Grant No. 2018/19943-6), for partial financial support. E.B.H. thanks CAPES for the financial support.

[1] Yu. E. Titarenko *et al.*, *INDC(CCP)-0447, IAEA Nuclear Data Section*, Vienna International Centre, A–1400, Vienna, Austria, October, 2009.
[2] Yu. E. Titarenko *et al.*, Phys. At. Nucl. **74**, 551 (2011).
[3] A. A. Kotov, L. A. Vaishnene, V. G. Vovchenko *et al.*, Phys. Rev. C **74**, 034605 (2006).
[4] J. Hudis and S. Katcoff, Phys. Rev. C **13**, 1961 (1976).
[5] V. I. Yurevich *et al.*, Phys. At. Nucl. **65**, 1383 (2002).
[6] R. Michel *et al.*, Nucl. Instrum. Methods Phys. Res. B **129**, 153 (1997).
[7] M. C. Duijvestijn, A. J. Koning, J. P. M. Beijers, A. Ferrari, M. Gastal, J. van Klinken, and R. W. Ostendorf, Phys. Rev. C **59**, 776 (1999).
[8] A. R. Balabekyan, N. A. Demekhina, G. S. Karapetyan *et al.*, Phys. Rev. C **90**, 054612 (2014).
[9] A. R. Balabekyan, N. A. Demekhina, G. S. Karapetyan *et al.*, Phys. Rev. C **89**, 054604 (2014).
[10] A. R. Balabekyan, N. A. Demekhina, V. M. Zhamkochyan, and G. S. Karapetyan, Phys. At. Nucl. **77**, 31 (2014).
[11] E. Andrade-II, G. S. Karapetyan, A. Deppman *et al.*, J. Phys. G: Nucl. Part. Phys. **45**, 015105 (2018).
[12] G. S. Karapetyan, A. R. Balabekyan, N. A. Demekhina, and J. Adam, Phys. At. Nucl. **72**, 911 (2009).
[13] A. R. Balabekyan, G. S. Karapetyan, N. A. Demekhina *et al.*, Phys. At. Nucl. **73**, 1814 (2010).
[14] A. Deppman *et al.*, Phys. Rev. C **88**, 064609 (2013).
[15] R. Michel *et al.*, J. Nucl. Sci. Tech. **39**, 242 (2002).
[16] R. B. Firestone, in *Tables of Isotopes*, 8th ed., 1998 update (with CD ROM), edited by S. Y. Frank Chu (CD-ROM editor) and C. M. Baglin (Wiley Interscience, New York, 1996).
[17] G. S. Karapetyan, Eur. Phys. J. Plus **130**, 180 (2015).
[18] H. Kudo, M. Maruyama, M. Tanikawa, T. Shinozuka, and M. Fujioka, Phys. Rev. C **57**, 178 (1998).

[19] A. V. Prokofiev, Nucl. Instrum. Methods Phys. Res. A **463**, 557 (2001).
[20] Y. Yariv and Z. Fraenkel, Phys. Rev. C **20**, 2227 (1979).
[21] T. Fukahori, O. Iwamoto, and S. Chiba, in *Proceedings of the 7th International Conference on Nuclear Criticality Safety, ICNC 2003, AERI-conf, 2003-019 (pts. 1-2)* (Japan Atomic Energy Research Institute, Tokaimura, Japan, 2003), p. 144.
[22] B. Schroder, G. Nydahl, and B. Forkman, Nucl. Phys. A **143**, 449 (1970).
[23] C. Chung and J. J. Hogan, Phys. Rev. C **25**, 899 (1982).
[24] A. Deppman, S. B. Duarte *et al.*, J. Phys. G: Nucl. Part. Phys. **30**, 1991 (2004).
[25] M. Gonçalves, S. de Pina, D. A. Lima, W. Milomen, E. L. Medeiros, and S. B. Duarte, Phys. Lett. B **406**, 1 (1997).
[26] S. de Pina, E. C. de Oliveira *et al.*, Phys. Lett. B **434**, 1 (1998).
[27] A. Deppman, O. A. P. Tavares *et al.*, Comput. Phys. Commun. **145**, 385 (2002).
[28] A. Deppman, O. A. P. Tavares, S. B. Duarte, J. D. T. Arruda-Neto, M. Gonçalves, V. P. Likhachev, and E. C. de Oliveira, Phys. Rev. C **66**, 067601 (2002).
[29] A. Deppman, G. Silva, S. Anefalos, S. B. Duarte, F. Garcia, F. H. Hisamoto, and O. A. P. Tavares, Phys. Rev. C **73**, 064607 (2006).
[30] I. González, F. Guzmán, and A. Deppman, Phys. Rev. C **89**, 054613 (2014).
[31] E. Andrade-II, I. González, A. Deppman, and C. A. Bertulani, Phys. Rev. C **92**, 064903 (2015).
[32] J. Cugnon, Th. Aoust *et al.*, Adv. Space Res. **40**, 1332 (2007).
[33] V. Weisskopf, Phys. Rev. **52**, 295 (1937).
[34] J. Pearson, Hyperfine Interactions **132**, 59 (2001).
[35] I. Dostrovsky, P. Rabinowitz, and R. Bivins, Phys. Rev. **111**, 1659 (1958).
[36] N. Bohr and J. A. Wheeler, Phys. Rev. **56**, 426 (1939).
[37] R. Vandenbosch and J. R. Huizenga, *Nuclear Fission* (Academic Press, New York, 1973).
[38] J. R. Nix, Rev. Nucl. Sci. **22**, 65 (1972).
[39] V. V. Pashkevich, Nucl. Phys. A **169**, 275 (1971).
[40] U. Brosa, S. Grossman, and A. Muller, Z. Naturforsch. A **41**, 1341 (1986).